INVESTIGATION OF SPENT REFRACTORY LINING IN AN ANODE BAKING FURNACE

Trond Brandvik[1], Zhaohui Wang[1,2], Arne Petter Ratvik[2] and Tor Grande[1]

1. Department of Material Science and Engineering, Norwegian University of Science and Technology, Trondheim, Norway
2. SINTEF Materials and Chemistry, Trondheim, Norway
Corresponding author: trond.brandvik@ntnu.no

Keywords: Anode baking furnace, refractory lining, degradation mechanism, chemical reactions.

Abstract

The refractory lining in anode baking furnaces is exposed to harsh chemical environment and thermal cycling. Spent refractory lining from an anode baking furnace after 4000 days in operation was investigated. Variation in the density and porosity across the bricks revealed that carbon build up in pores had taken place towards the anode side. The spent refractory bricks were investigated with respect to chemical and mineralogical composition by X-ray diffraction and electron microscopy. No significant change in the mineralogical composition across the brick could be detected by X-ray diffraction. Fluoride was not found in the bricks, while traces of sodium was shown to accumulate together with other impurities in the bricks. The changes in the chemical and mineralogical composition across the bricks are discussed in relation to possible chemical reactions taking place during anode baking.

Introduction

An important part in the process of aluminum electrolysis are the production and quality of the pre-baked carbon anodes, where the main production principle is quite similar from plant to plant [1–3]. The most significant variation with respect to furnace design is whether the furnace has an open or closed top section [4]. A mixture of coke and anode butts is crushed, mixed with pitch and formed into green anodes, which are subsequently heat treated in the anode baking furnace. In the electrolysis cell, as the anodes reaches 20-25 % of their original size, they are taken out of operation and recycled to the production of green anodes. The use of recycled anodes reduces both anode costs and the use of the carbon materials. Due to the exposure to cryolite and anode cover materials during electrolysis, recycled anodes constitute a source of impurities, especially sodium and fluorine from the bath, that normally is not found in great amounts in the anode raw materials [1,5]. In the anode-baking furnace, aluminosilicate refractory walls are used to separate the anodes from the hot flue gas. During a baking cycle, typically lasting 20-30 days, the temperature varies from ambient to about 1200-1300 °C. Due to the high temperature, cryolite contaminations in the anodes will evaporate forming gaseous NaF and $NaAlF_4$. The combination of thermal cycling and chemically harsh environments results in refractory degradation and eventually the need for the refractory wall to be replaced [3,6].

Investigations of degradation of refractory lining in anode baking furnaces have been reported in several works [1–3,6]. These investigations have shown mineralogical changes close to the anode side of the refractory, in addition to blackening of the refractory caused by carbon deposition. Gaseous sodium and fluorides were proposed to react with the lining forming a liquid phase, which during cooling forms a glass phase with a lower solidus temperature compared to the original refractory lining [1–3]. This mechanism causes the thermomechanical properties of the refractory lining to change, which eventually leads to deformation and degradation of the lining. The interaction of similar materials with sodium aluminum fluorides has also been studied in depth in relation to the refractory lining in electrolysis cells [1–3,6–16].

Materials from an autopsy of a flue wall after approximately 4000 days in operation were characterized in this work. The density and porosity variations in the outer layers facing the anodes are linked to the deposition of carbon in the open porosity. Changes in phase composition were evaluated as a function of distance from the anode and compared to similar findings from previous investigations on anode baking furnaces. Reaction mechanisms describing the degradation are discussed.

Method

Materials from a spent refractory lining were collected from an open top anode baking furnace after approximately 4000 days in operation. Samples were taken from three positions on the refractory wall (high, middle and low) and named H, M and L, respectively. The uppermost sample is collected approximately 1 m from the top of the furnace. All samples were collected approximately 1 m from the pit cross wall. Figure 1 shows a typical cross section of a refractory sample. The darker region on the left hand side is facing the anode pit, and the bright area at the right hand side is facing the flue. The interface between the dark and bright regions was observed to vary with sampling position. The samples were divided into sections, named a to h according to the sampling presented in Figure 1. In addition to the full width sampling, two narrow samples were also collected as shown in Figure 1.
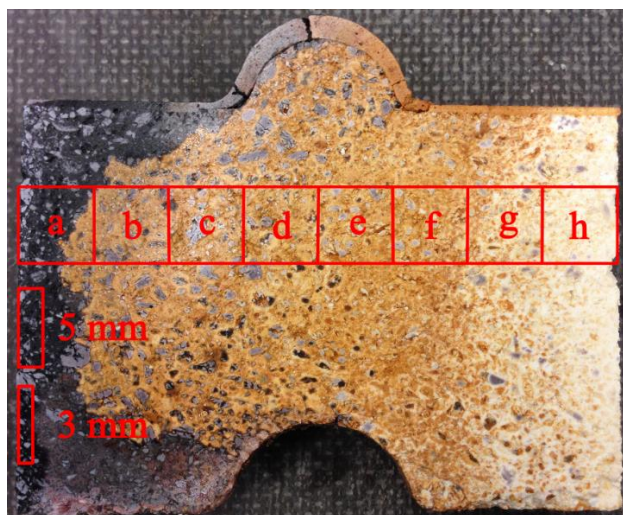

Figure 1. The cross section of a typical sample of exposed refractory lining. The anode pit side is to the left and the flue side is to the right of the brick. The full width sampling with

the associated nomenclature has been the basis for most of the investigations in this work. In addition, samples of 3 and 5 mm thickness have been prepared for carbon content analysis.

Density and porosity measurements were carried out using the Archimedes' method in accordance with ISO5017. Mineralogical analysis through X-ray diffraction was conducted on a Bruker D8 Focus diffractometer with a LynxEye SuperSpeed detector. Chemical analysis was carried out with a Hitachi S-3400N scanning electron microscope (SEM), with the associated energy dispersive X-ray spectroscopy (EDS). In addition, X-ray fluorescence analysis were carried out with a Bruker S8 Tiger 4 kW X-ray diffractometer.

Results

The refractory material used in the anode baking furnace has a highly heterogeneous microstructure, with dense aggregates (ranging from micron range to several millimeters in size), bonded together by a fine matrix phase as shown in Figure 2. The measured chemical composition and some physical data of the pristine material are presented in Table 1.
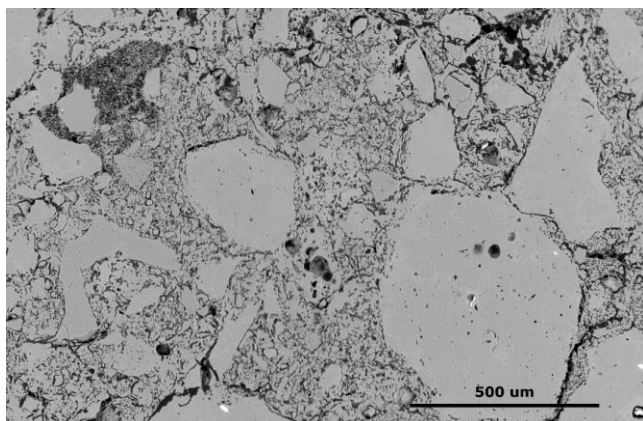

Figure 2. Micrograph of the pristine unreacted refractory material.

Table 1. Chemical composition and some physical properties for the pristine material.

Specie	Wt%
Al_2O_3	51
SiO_2	46
TiO_2	1.5
Fe_2O_3	1
K_2O	0.2
CaO	0.2
Density	2.4 gcm^{-3}
Open porosity	15 vol%

X-ray diffractograms for sample L with full width sampling (a-h) are displayed in Figure 3, where mullite ($Al_6Si_2O_{13}$) and cristobalite (SiO_2) are found to be the main phases. The overall change in phase composition with respect to distance from the anode side is minor according to the X-ray patterns. The same is observed for samples H and M. However, when focusing on the broad strong reflection highlighted in Figure 3, there are some significant variations worth mentioning. As the distance from the anode increases (going from a to h), there is a clear variation in the intensity and the position of

the reflection attributed to cristobalite (located at 2θ=21.9°). It is also most likely that the reflection consists of three reflections where only one can be assigned to cristobalite. The variations do, however, not proceed as a linear function of the distance from the anode. For samples L-a to L-e, the broad middle reflection decreases in intensity and the reflection assigned to cristobalite increases, while from L-f to L-h the trend is reversed. This variation is observed to a similar degree for sample M, while it is not very pronounced for sample H. The shift appears at approximately 6-7.5 cm into the wall. Apart from the minor intensity shift in the highlighted peaks in Figure 3, there is no significant variation in the overall phase composition.
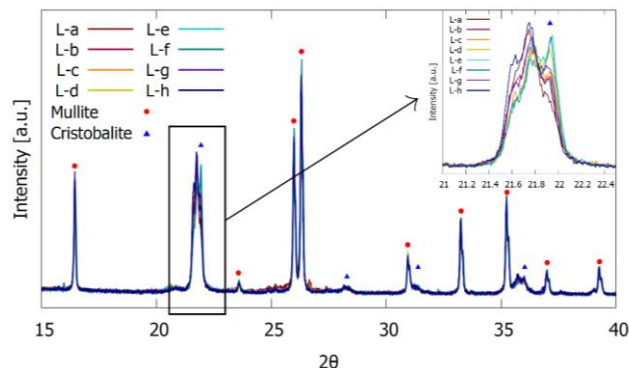

Figure 3. X-ray patterns for sample L as a function of distance from the anode.

Measurements of the density and the porosity for samples L, M and H were carried out across the whole brick in accordance to the sectioning presented in Figure 1. The samples were then heat treated in air at 1150 °C for 48 hours, before the measurements were repeated. The results for sample L are presented in Figure 4, showing almost no change in density and porosity due to the heat treatment. The blue dotted line indicates the pristine density, which is in good agreement with the four measurements closest to the burner side. Closer to the anode, the density increases before it drops for the outermost layer. The same behaviour is observed for sample M.
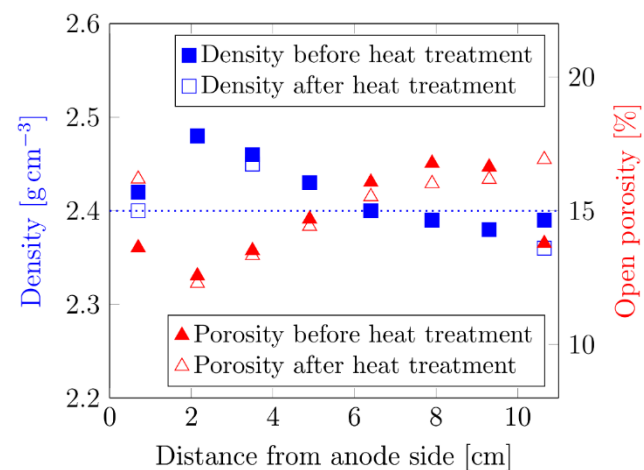

Figure 4. Density and open porosity for sample L as a function of distance from the anode side is plotted before and after heat treatment. The density of the pristine material is indicated by the blue dotted line.

The measured density and porosity of sample H is presented in Figure 5. These results show density changes in the samples closest to the anodes caused by heat treatment, compared to the results in Figure 4. The density of the sample closest to the anode side is the only sample clearly affected by the heat treatment, while the others are more or less unaffected. After heat treatment, the data show a similar trend as observed for samples M and L, with an increased density at samples H-b to H-d. The difference between the baseline (the density level closest to the flue) and the highest data point is, however, not as pronounced as for samples M and L. It is also observed that the density baseline for sample H is found around 2.35 gcm^{-3}, which is lower than the pristine density observed for sample M and L.
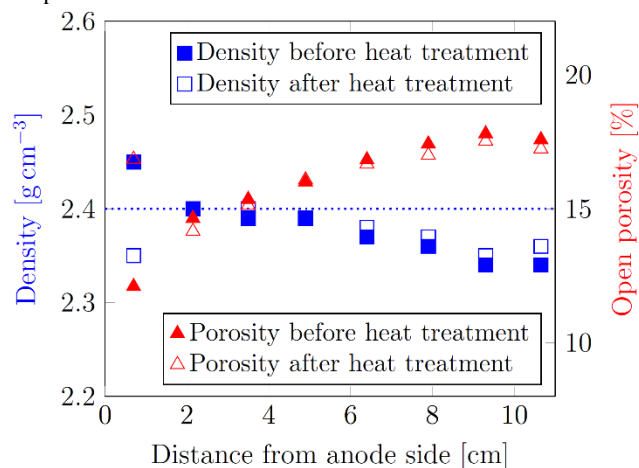

Figure 5. Density and open porosity for sample H as a function of distance from the anode side plotted before and after heat treatment. The density of the pristine material is indicated by the blue dotted line.

Sample sectioning shown before and after the heat treatment procedure is presented in Figure 6. The blackening of the samples is almost completely removed due to the heat treatment. Measurements of weight loss during heat treatment showed a weight loss of 4 wt% for the sample closest to the anode side, while no significant weight loss during heat treatment was measured for the other samples.

Figure 6. Samples before (upper) and after (lower) heat treatment. The samples closest to the anode side were clearly blackened during operation in the anode baking furnace.

Figure 7 show a comparison of the X-ray patterns of samples with 3 and 5 mm width, a coke sample and the pristine, unexposed material. The indicated widths are measured from the anode-facing surface and into the refractory wall. The green line in Figure 7 show the main reflection related to the coke sample. The pristine material has naturally no significant coke content, while the exposed samples do show considerable amounts of coke in the outer layers of the sample. As the width of the exposed sample decreases, the

amount of coke in the sample becomes more significant. The carbon content in the 3 mm sample is thus higher than the sample with 5 mm thickness.
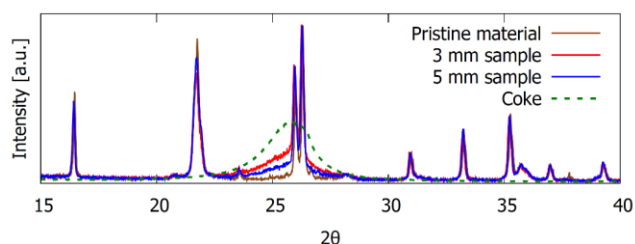

Figure 7. Comparison of pure carbon with thin exposed refractory samples and the pristine unexposed material.

As shown in Figures 4 and 5, the refractory material has a substantial amount of open porosity (10-20 %). Consequently, gaseous species can diffuse into the material increasing the amount of exposed refractory surface. When investigating the outer layers of the most exposed samples (H-a, M-a and L-a), there are clear signs of chemical wear on some of the grain surfaces. The SEM image in Figure 8 show an overview of sample L-a with the anode-facing surface pointing upwards.
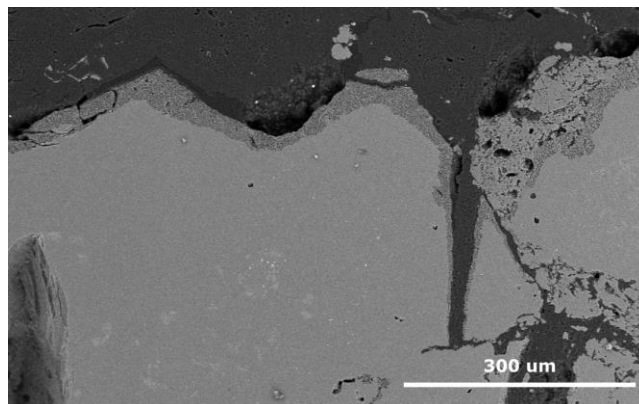

Figure 8. Overview of the exposed sample L-a with the anode-facing surface pointing upwards. The outer layers of the grains are clearly affected by years in operation.

The sample in Figure 8 consist mostly of larger grains with some porosity in between. The outer layers of the grains facing the anodes are clearly affected by years in operation. Figure 8 show a 50-100 µm thick layer on the grains where both the microstructure and the chemical composition of the structure are changed. A part of the affected region is shown in greater detail in Figure 9, where the dense grain is found in the lower part of the figure, while the affected region consists of a less dense, rod-like microstructure. The grains of the dense bulk phase are more or less the same as found in the pristine material. There is no significant increase in Na content in the exposed regions, compared to the Na content in the pristine material. The distribution of Al, Si, O and C is measured by EDS mapping and presented in Figure 10. The EDS analysis show a change in chemical composition from the dense bulk region to the affected porous areas of the grains. At the boundary between the dense and porous parts of the grain, there is an abrupt change in the silicon level.
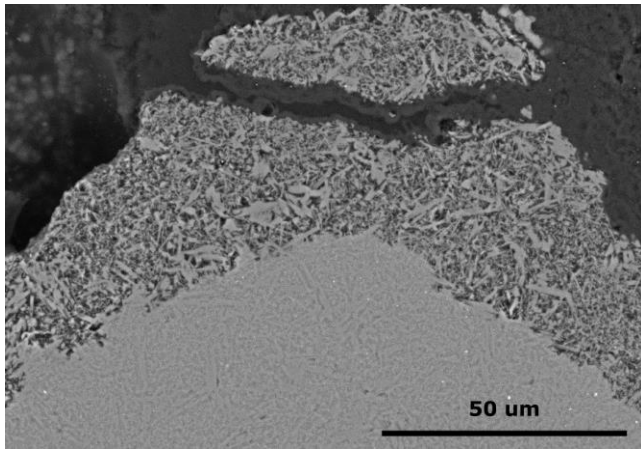
Figure 9. Detailed micrograph of the region of the materials in Figure 8 where mineralogical transformations are evident. The anode-facing surface is pointing upwards.

The reacted region is almost depleted of silicon, while the aluminum oxide is left in the structure. The amount of aluminum and oxygen is however more or less constant throughout the investigated region. The chemical wear is observed throughout the outer layers of the samples, but seems to be varying with both sampling position in the furnace and distance into the refractory away from the anode side.
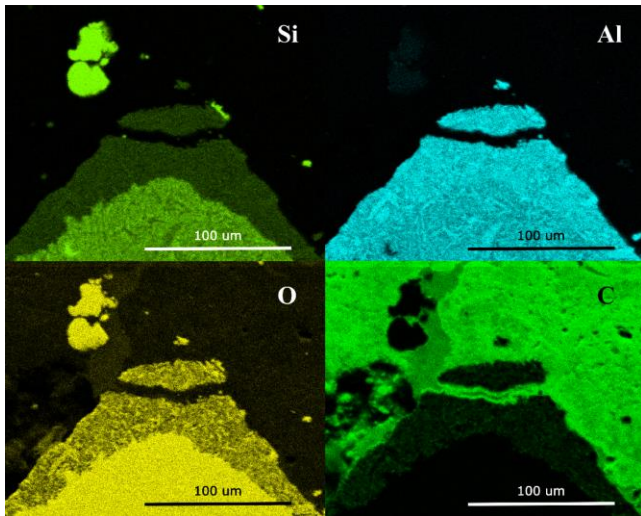

Figure 10. Element distribution in the surface region of sample L-a presented in Figure 9. The anode-facing surface is pointing upwards.

There are indications of increased degradation in the bottom of the pit compared to the upper regions, i.e. sample L-a is more affected than H-a. The thickness of the affected porous region is decreasing as the distance from the anodes is increasing. Chemical degradation is also found at the inside of pores several millimetres into the refractory.

Figure 11 and Figure 12 present sample H-a with the anode-facing surface pointing upwards. This sample is collected from the top section of the furnace, showing minor signs of chemical wear. Sphere-like particles of SiO_2 are on the other hand observed in the immediate vicinity of the refractory at the anode side. These particles are found all over the refractory surface on sample H-a.

The samples collected further down in the furnace, samples M and L, show no signs of such particles. From Figure 12 there are signs of impurities (Na and K) and Al in the SiO_2 rich particles. This suggests that the particles are not crystalline SiO_2, but rather an amorphous glassy phase where the solubility of impurities are higher.
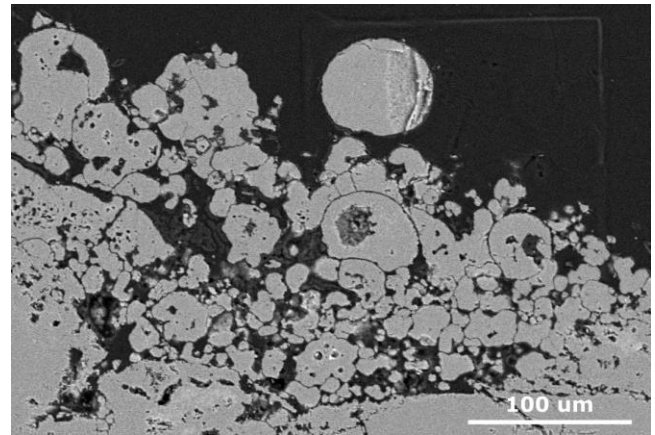

**Figure 11. Surface region of sample H-a with the anode-facing surface pointing upwards.**
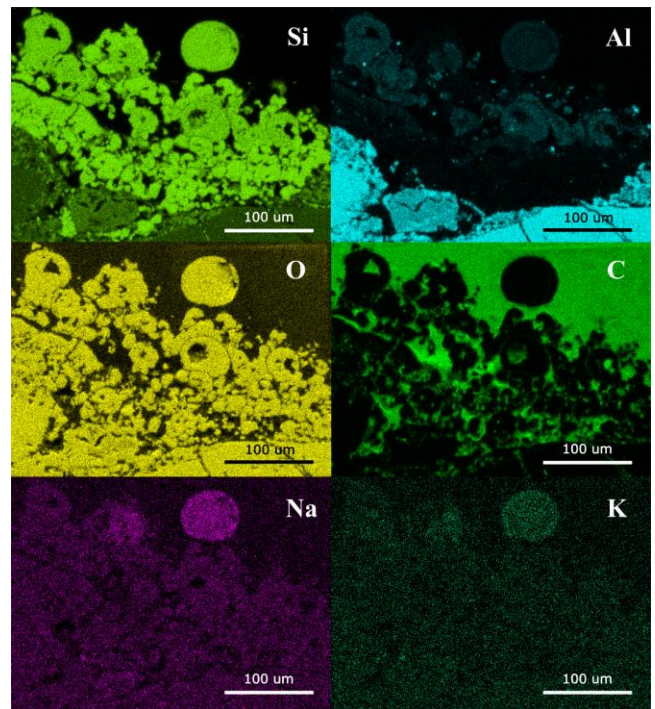
Figure 12. Element distribution in the surface region of sample H-a close to the anode side. The anode-facing surface is pointing upwards.

Discussion

The density variations presented in Figure 4 demonstrate that the macrostructure of the wall has changed towards the anode side. Close to the burner side, the measured density equals the pristine density (the baseline), while it increases closer to the anode. The difference between the maximum measured density and the baseline is approximately 3-4 % for samples M and L. The same

behaviour is observed for the heat treated H samples presented in Figure 5, however with a baseline at around 2.35 gcm^{-3}. The difference between the maximum measured density and the baseline is found to be approximately 2 %. The density variations are thus found to be greater in the middle and bottom of the pit, compared to the top section. The fact that X-ray diffraction analysis does not detect significant compositional variations, points to the formation of an amorphous phase or densification of the refractory.

The chemical wear observed in the middle and bottom section of the pit show regions with pronounced SiO_2 depletion. The chemical wear is, however, only observed at the surface of the grains closest to the anode. These observations correspond with the assumption that volatile species are entering the structure through the open porosity, and react with the outer layers of the grains. The partial pressure of the reacting species is decreasing with increasing distance from the anode, leading to a reduction in chemical wear on the grains. Brunk [6] reports on SiO_2 depletion from refractory materials in anode baking furnace similar to the observation in this work. He explained the observation with the reduction of SiO_2 by CO, as presented in Equation 1.

$$SiO_2(s) + CO(g) = SiO(g) + CO_2(g) \qquad (1)$$
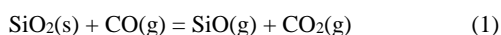
At elevated temperatures, the partial pressure of CO in the anode baking furnace becomes high enough to favour the formation of gaseous SiO [6]. Samples collected from the lower (sample L) and middle (sample M) section of the furnace show pronounced chemical wear in the outer layers, while this is not observed to the same extent in the samples collected from the top section (sample H) of the furnace. The anode baking furnace investigated in this work has an open top configuration, and it could be assumed that the partial pressure of oxygen is higher in the upper parts of the oven, compared to the bottom. The atmosphere in the top section is thus less reducing, preventing the reduction of SiO_2 to take place.

EDS analysis of the SiO_2 depleted regions shows a chemical composition close to the mullite composition. The average composition of the dense unreacted regions does on the other hand correspond to andalusite (Al_2SiO_5) and SiO_2 in a 50/50 atomic ratio. Andalusite is often used as a precursor in the production of refractory materials [6]. During heat treatment, the thermodynamically unstable andalusite decomposes into mullite and SiO_2 according to Equation 2.

$$3Al_2SiO_5(s) = Al_6Si_2O_{13}(s) + SiO_2(s) \qquad (2)$$
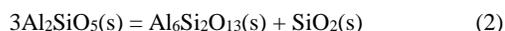
After decomposition, the material ends up with a matrix of rod-like mullite particles with SiO_2 filling the voids, denoted mullitised andalusite [3,17]. The heat treated refractory material is thus consisting of a combination of mullite and SiO_2, corresponding to the X-ray analysis presented in Figure 3. As SiO_2 is reduced and removed from the structure, only the mullite matrix is left, as shown in Figure 9.

The measured density for sample H shows a significant variation prior to and after heat treatment for the samples closest to the anode. This reduction in density is attributed to the removal of carbon during heat treatment. The X-ray patterns presented in Figure 7 demonstrate the presence of carbon in the outer layers of the refractory. The closer to the surface (thinner samples), the more significant the carbon content becomes. These investigations demonstrate clearly that carbon is deposited in the open porosity of

the refractory bricks during operation in the anode baking furnace. During heating, gaseous CO and volatile hydrocarbons from the green anodes are transported to the vicinity of the refractory. Carbon deposition could thus be a result of carbon cracking at the refractory wall. Another possible source of carbon deposition is a reaction between gaseous SiO and CO_2, forming SiO_2 and carbon according to Equation 3.

$$SiO(s) + CO(g) = SiO_2(s) + C(s) \qquad (3)$$
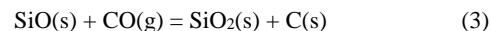
This reaction is a combination of the Boudouard reaction and the reversed reaction in Equation 1. As the temperature decreases in the last part of the temperature cycle, the CO/CO_2 gas mixture becomes unstable, shifting the Boudouard reaction, and the reaction in Equation 3, towards carbon deposition [18]. Evidence of carbon deposition has not been found in the middle and bottom section of the furnace, demonstrating that the amount of carbon deposition in the pores are not sufficient to influence the density measurements.

The fact that carbon is only oxidized and deposited in the upper parts of the furnace corresponds to the observation of SiO_2 deposition in the same sections. The reducing atmosphere is most pronounced in the bottom of the furnace and becomes less reducing further up. SiO_2 is reduced in the bottom of the furnace forming gaseous SiO, and transported upwards to the less reducing atmosphere. As the environment becomes sufficiently oxidizing, SiO is re-oxidized forming droplets of amorphous SiO_2 at the face of the refractory wall. Impurities like Na and K, in addition to Al, are observed in the SiO_2 particles. The presence of such impurities reduces the particles' viscosity, favouring the formation of spherical particles.

There are no signs of increased sodium or fluorine content in the exposed regions of the refractory, even though both $NaAlF_4$ and NaF are expected to be present in the gas phase of the furnace [18]. A recent thermodynamic study of potential reactions between volatile fluorides and the refractory wall, suggests refractory degradation could be caused by several thermodynamically possible reaction schemes [18]. Most of these reactions result in the formation of the sodium aluminosilicates; nepheline or albite. The fact that no significant levels of sodium has been observed in the spent lining, indicate that this is not the domination degradation mechanism in the present samples. The level of NaF and $NaAlF_4$ in the gas phase are too low for such reactions to dominate, most likely due to good cleaning routines of the anode butts, reducing the amount of bath entering the green anodes.

Conclusion

The present work has demonstrated that the dominating refractory degradation mechanism observed in open top anode baking furnaces are the reduction of SiO_2 by gaseous CO. The degradation is more pronounced in the middle and bottom section of the pit due to increased reducing atmosphere. The open top configuration leads to an increased partial pressure of oxygen in the top section of the furnace, where gaseous SiO is re-oxidized, forming spherical particles in the immediate vicinity of the refractory surface. Carbon is deposited at the wall in the upper part of the furnace. This is due to carbon cracking at the refractory wall, and a result of the oxidation of SiO. Combined with the increased density close to the anode side, the deposited carbon causes the thermomechanical properties of the refractory to change.

References

[1]   P. Prigent, M.L. Bouchetou, "Gaseous Corrosion of Alumino-Silicate Refractories in Anode Baking Furnaces used for Aluminium Produciton Part 1," *Interceram*, 58 (2009), 121–126.

[2]   P. Prigent, M.L. Bouchetou, "Gaseous Corrosion of Alumino-Silicate Refractories in Anode Baking Furnaces used for Aluminium Produciton Part 2," *Interceram*, 58 (2009), 202–209.

[3]   P. Prigent, M.L. et al., "The effect of the addition of fine andalusite particles in refractory bricks on gaseous corrosion," *JOM*, 60 (2008), 58–63.

[4]   F.H. Becker, F. Goede, "Ring Pit Furnaces for Baking of High Quality anodes - an Overview," *Aluminium 82*, 9 (2006).

[5]   A. Radjenović, "Properties of carbon anode components for aluminium production," *Nafta*, 63 (2012), 111–114.

[6]   F. Brunk, "Corrosion and Behavior of Firecal Bricks usen in the Flues of Open Anode Baking Furnaces," *Light Metals*, 1995, 641–646.

[7]   C. Schøning, T. Grande, O.-J. Siljan, "Cathode refractory materials for aluminium reduction cells," *Light Metals*, 1999, 231–238.

[8]   O.-J. Siljan, T. Grande, C. Schøning, "Refractories for aluminium electrolysis cells part 1 - Deterioration mechanisms based on phase equilibria," *Aluminium 77*, (2001), 294–300.

[9]   O.-J. Siljan, T. Grande, C. Schøning, "Refractories for aluminium electrolysis cells part 2 - Physical properties of penerating melt, reduction by metals and volatile fluorides," *Aluminium 77*, (2001), 385–390.

[10]   O.-J. Siljan, T. Grande, C. Schøning, "Refractories for aluminium electrolysis cells part 3 - Laboratory test for cryolite resistance," *Aluminium 77*, (2001), 610–615.

[11]   O.-J. Siljan, T. Grande, C. Schøning, "Refractories for aluminium electrolysis cells part 4 - Comparison of laboratory investigations and autopsies of pot linings," *Aluminium 77*, (2001), 809–814.

[12]   O.-J. Siljan, C. Schoning, T. Grande, "State-of-the-art alumino-silicate refractories for al electrolysis cells," *JOM*, 54 (2002), 46–55.

[13]   C. Schøning, T. Grande, "The stability of refractory oxides in sodium-rich environments," *JOM*, 58 (2006), 58–61.

[14]   K. Tschope et al., "Chemical Degradation of Cathode Linings in Hall-Heroult Cells - An autopsy Study of Three Spent Pot Linings," **Metall. Mater. Transcations B**, 43B (2012), 290–301.

[15]   K. Tschöpe, J. Rutlin, T. Grande, "Chemical Degradation Map for Sodium Attack in Refractory Linings," *Light Metals*, 2010, 871-876.

[16]   J. Butter, A. Bongers, "Alterations of Anode Baking Furnace Bricks During Operation," *Light Metals*, 1995, 633–639.

[17]   P. Prigent, M.L. Bouchetou, J. Poirier, "Andalusite: An amazing refractory raw material with excellent corrosion resistance to sodium vapours," *Ceramics Intternational*, 37 (7) (2011), 2287–2296.

[18]   T. Brandvik, A.P. Ratvik, T. Grande, "Thermodynamic Assessment of the Chemical Durability of Refractory Lining in Anode Baking Furnaces," ICSOBA, 2016.